Engineering upconversion emission spectra using plasmonic nanocavities

Christopher Lantigua,[1] Sha He,[2] Milad Akhlaghi Bouzan,[1] William Hayenga,[1] Noah J. J. Johnson,[2] Adah Almutairi,[2] and Mercedeh Khajavikhan[1,*]

[1]*CREOL, College of Optics and Photonics, University of Central Florida, Orlando, Florida 32816-2700, USA*

[2]*Skaggs School of Pharmacy and Pharmaceutical Sciences, KACST-UCSD Center of Excellence in Nanomedicine, Laboratory of Bioresponsive Materials, University of California, 9500 Gilman Dr., 0600, PSB 2270, La Jolla, San Diego, California 92093, USA*

**Corresponding author: mercedeh@creol.ucf.edu*

Received April 11, 2014; revised May 20, 2014; accepted May 20, 2014; posted May 23, 2014 (Doc. ID 209223); published June 16, 2014

We show that the upconversion emission spectra of Tm^{3+} and Yb^{3+} codoped β-$NaYF_4$–$NaYF_4$ core-shell nanoparticles can be judiciously modified by means of plasmonic nanocavities. Our analysis indicates that more than a 30-fold increase in conversion efficiency to the UV spectral band can be expected by engineering the NIR absorption and the local density of states. The effect of the nanocavity on the resulting radiation patterns is discussed. Our results are exemplified in cylindrical cavity geometries.

OCIS codes: (190.7220) Upconversion; (240.6680) Surface plasmons; (310.6628) Subwavelength structures, nanostructures; (260.3800) Luminescence.

http://dx.doi.org/10.1364/OL.39.003710

Photon upconversion (UC) is an anti-Stokes process in which the sequential absorption of two or more photons leads to the emission of light at a shorter wavelength. Materials for which UC can take place often contain ions of d-block and f-block elements [1,2]. In recent years, upconversion nanoparticles (UCNPs) have attracted considerable attention due to their potential applications in a number of areas such as bio-imaging, photovoltaics, drug delivery, and therapeutics, to name a few [3]. These applications have motivated research toward developing more efficient UC materials. For example, significant progress has been made in synthesizing codoped UC nanocrystals in which one type of doping (sensitizer) absorbs the radiation and transfers it to another type of doping (activator). Furthermore, the quenching through surface defects and nonradiative recombination has been substantially subdued by appropriately shelling the upconverting nanocrystals [4]. Despite these advancements, the low luminescence efficiency still remains a limiting factor for UC systems.

The efficiency of UC processes for each nanoparticle alone is mainly governed by chemistry and synthesis techniques. However, in applications where several upconverting nanoparticles can be encapsulated in submicrometer size cavities, photonics and quantum optics can provide appropriate tools to further customize their emission spectra and radiation patterns. For example, a threefold enhancement of near-infrared (NIR) absorption has been reported using gold nanoparticles in conjunction with Er^{3+} doped $NaYF_4$ UCNPs [5]. In addition, metallic patterning schemes have been suggested as ways to increase NIR absorption of UC nanocrystals [6–8], but the emission in such structures is subject to quenching, since UCNP are placed in close proximity to metals.

In this Letter, we show that nanoscale metal cavities can be utilized to increase the efficiency of the UC processes by more than an order of magnitude. Our analysis is carried out for amalgams of β-phase $NaYF_4$: Yb^{3+}, Tm^{3+}–$NaYF_4$ core-shell nanoparticles encapsulated in a cylindrical plasmonic nanocavity. In this case, the presence of the nanocavity alters the absorption characteristics as well as the local density of states (LDOS). The resulting effects are then incorporated into the rate equation model, which in turn dictates the emission spectrum. Finally, the impact of these nanocavities on the emission directionality of the UC systems is discussed.

Figure 1 depicts the geometry of the system to be analyzed. The UCNP are embedded in a thin film of a polymer host with a matching refractive index of $n = 1.5$ [9]. UC containing nanocavities are then formed by patterning cylindrical rods, which are subsequently shelled by aluminum tubes, as shown in Fig. 1. Since the UCNPs dispersed in the polymer film are well separated from the metallic tube, this arrangement is less susceptible to quenching. This UC containing cylinder nanocavity is assumed to have a radius of 150 nm and a height of 200 nm. In our analysis, the radial thickness of the aluminum tube is taken to be 50 nm. This thickness can be larger without having a noticeable effect on the results presented in this study. The goal here is to maximize the conversion from the NIR band to the ultraviolet (UV) band. To this end, aluminum has been selected, since it has a lower

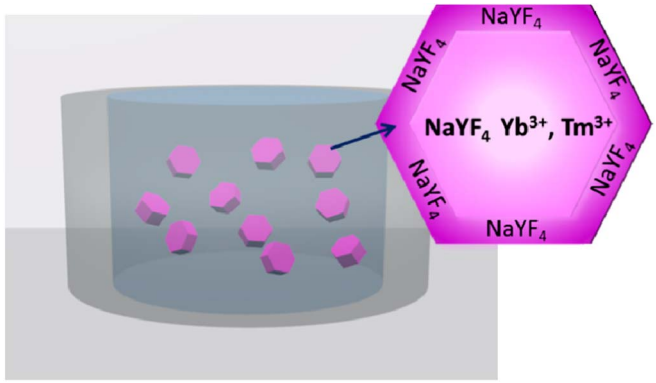

Fig. 1. Schematic of the nanocavity containing UC β-phase $NaYF_4$: Yb^{3+}, Tm^{3+}–$NaYF_4$ core-shell nanoparticles.

dissipation loss at UV bands in comparison with other plasmonic metals such as gold and silver. In certain other applications in which the aim is to increase the conversion efficiency to visible, gold and silver tubes can be more appropriate choices.

Since UC is a nonlinear process, increasing the NIR absorption (effectively increasing the incident power delivered to the nanoparticles) can improve the conversion efficiency to all spectral bands. The ground state absorption (GSA) of the activator ions, as well as the excited state absorption (ESA), and stimulated emission (STE) processes in the sensitizer ions linearly scale up with the incoming photon flux density. These in turn influence the overall dynamics of the UC system.

The analysis for the absorption of the 980 nm NIR excitation is carried out using finite element methods (FEM). The net absorption coefficient of the polymer containing UCNPs is taken to be 5 cm^{-1} [5]. Figure 2 compares the NIR absorption from a bare cylinder [Fig. 2(a)] to that of the aluminum-tubed cylinder [Fig. 2(b)]. In these figures, the absorption profile is provided as a function of spatial cylindrical coordinates r and z. In both cases, the capsules are illuminated by a linearly polarized plane wave, which is incident from the bottom. For the aluminum-shelled structure, the FEM simulation predicts an overall enhancement factor (the polymer containing UCNP region) of more than three in the absorption in comparison with the unshelled cylinder.

The proposed plasmonic shielding also alters the LDOSs at the resonant transition frequencies of the sensitizer. The transition probability P_{if} of the spontaneous emission process at a frequency ω_{if} is governed by Fermi's golden rule and is directly proportional to the LDOSs $\rho(\vec{r}, \omega_{if})$ at position $\vec{r}$ and is given by

$$P_{if}(\vec{r}, \omega_{if}) = \frac{2\pi}{\hbar} |M_{if}|^2 \rho(\vec{r}, \omega_{if}), \quad (1)$$

where M_{if} represents a dipole transition matrix element [10]. Since the output luminescence at frequency ω_{if} is linearly proportional to the rate of the associated transition, in principle, by engineering the LDOS, one can fine tune the transition rates in order to increase the UC quantum yield at the spectral band of interest.

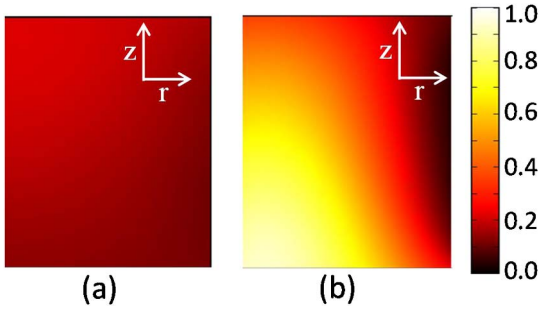

Fig. 2. Normalized absorbed power density (watt per volume) at a wavelength of 980 nm (NIR) in the polymer region by (a) UCNPs embedded in a bare cylindrical cavity. (b) The same structure when surrounded by an aluminum ring with a thickness of 50 nm as depicted in Fig. 1.

In Fig. 3, FEM results for the enhancement of LDOS in the two aforementioned UC systems are presented. The simulations are performed for an ensemble of 10 randomly oriented dipoles, placed in random locations within the polymer cylinder. Figure 3 shows that, while the bare cylinder exhibits no marked features, the aluminum-shelled structure displays more than an 11-fold improvement in the LDOSs at the UV spectral band centered at 360 nm.

Through the above two mechanisms, the proposed nanoscale plasmonic cavity alters the dynamical response of the UCNP. This can be modeled by employing a set of rate equations adapted to these systems. The rate equations to these $NaYF_4$: Tm^{3+}, Yb^{3+} based systems are given as

$$\dot{n} = (M_{GSA} + M_{ESA} + M_{STE} + M_{MP} + M_{SPE})n + [ET], \quad (2)$$

where vector n represents populations of the involved energy bands, which includes $^2F_{7/2}$ and $^2F_{5/2}$ levels of the activator (Yb^{3+}) ions, and $^3H_6$, $^3F_4$, $^3H_5$, $^3H_4$, $^3F_2$ & $^3F_3$, $^1G_4$, $^1D_2$ levels of the sensitizer (Tm^{3+}). The GSA matrix (M_{GSA}) describes transitions between $^1F_{7/2}$ and $^1F_{5/2}$ of the activator ions, and similarly the ESA matrix (M_{ESA}) dictates the transitions between the sensitizer's upper levels with energy separation corresponding to the excitation frequency. The STE (M_{STE}) matrix represents the rate of stimulated transitions at the excitation wavelength of 980 nm. The multiphonon matrix (M_{MP}) accounts for the nonradiative transitions between energy bands enabled by multiple phonons exchanged between the host crystal and the sensitizer ions. Finally, the spontaneous emission matrix (M_{SPE}) represents the spontaneous radiative transitions between all energy bands involved. In addition to the above linear processes, a total of eight nonlinear processes are considered in our model, which governs the energy transfer between the sensitizer and activator ions ([ET]). Half of these processes are UC energy transfers, while the other half are cross-relaxation mechanisms. The energy transfer between activator and

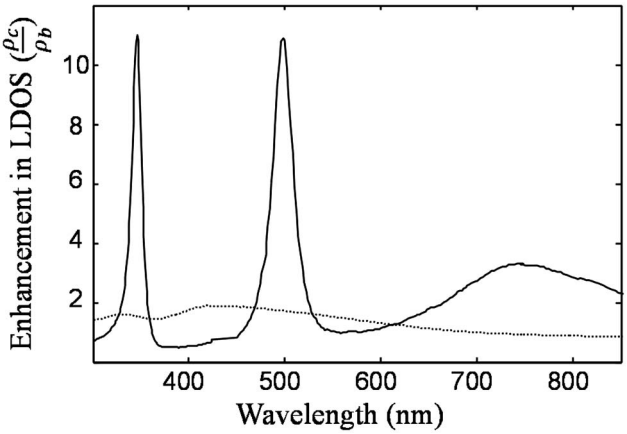

Fig. 3. Enhancement factor of the LDOS for UCNPs embedded in a bare polymer cylindrical cavity (dashed line) and for the same structure when surrounded by an aluminum ring with a thickness of 50 nm (solid line). ρ_b and ρ_c are the LDOSs in the bulk and in the cavity, respectively.

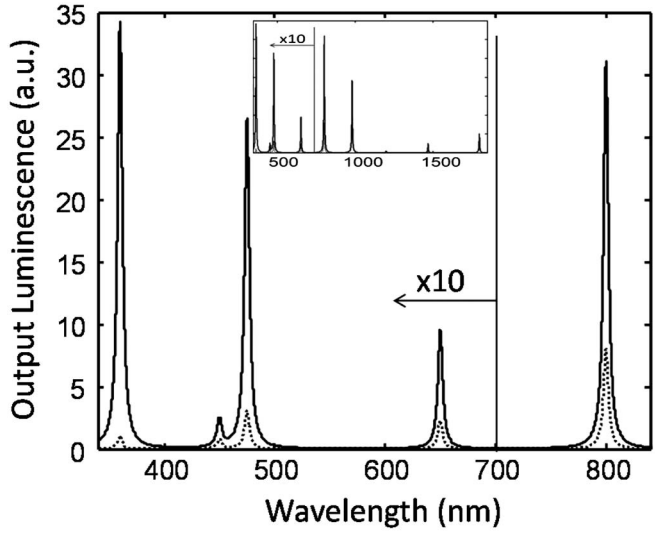

Fig. 4. Spectrum of the $NaYF_4$: Tm^{3+}, Yb^{3+} UCNP. The dotted line represents the luminescence spectrum of UCNPs in a polymer rod, while the solid line depicts the luminescence spectrum of UCNPs in the aluminum-tubed nanocavity of Fig. 1. The inset shows the full spectrum (340–1840 nm). Below 700 nm, the emission is magnified by an order of magnitude to facilitate visual comparisons.

sensitizer ions originates from the near-field dipole-dipole interactions. The parameters used in our analysis are extracted from available literature [11–13].

The rate equation system is integrated using a Runge–Kutta method numerically. Other numerical techniques may also be employed by applying the steady-state condition ($\dot{n} = 0$) to turn the system of differential equations into a system of algebraic equations. The output luminescence at the frequency of interest is then calculated by multiplying the population of an initial level with the decay rate associated with the corresponding final level. Using this technique, it is possible to find the full emission spectrum of UC nanoparticle systems. Figure 4 shows the spectrum of the two previously mentioned $NaYF_4$: Yb^{3+}, Tm^{3+}–UCNP systems. The dotted line represents the luminescence spectrum of nanocrystals in the polymer rod while the solid line depicts the luminescence spectrum of UCNPs in the aluminum-tubed nanocavity of Fig. 1. As shown in this figure, the inclusion of the nanocavity results in a 34-fold increase in the luminescence emission at the targeted UV spectral band centered at 360 nm. The simulation is performed for an excitation intensity of 1000 W/m^2 with a spectral broadening of 2.6 nm at a wavelength of 980 nm. All emission signatures corresponding to the resonant transition frequencies in the Tm^{3+} and Yb^{3+} are assumed to have an identical Lorentzian line shape, while the transition probability is only affecting the peak values. The doping concentration of Tm^{3+} and Yb^{3+} ions is 0.3% and 25%, respectively.

In addition to improved UC efficiency at the desired spectral band, placing UCNPs in judiciously designed nanocavities can tailor their radiation pattern. Figure 5 shows the spatial structure of the electromagnetic (optical) mode supported by the above cavity at a wavelength of 360 nm. The quality factor of this mode is 21. No

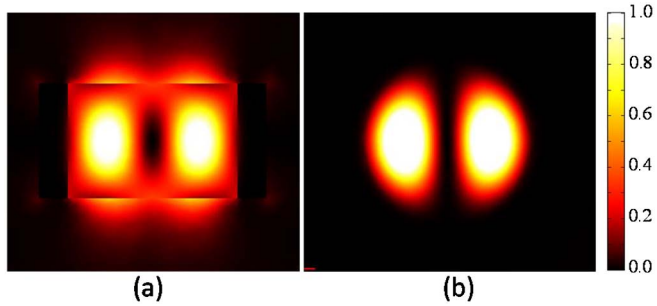

Fig. 5. Confined electromagnetic mode in the UCNP-polymer system surrounded by an aluminum tube. The cavity supports a plasmonic mode with a quality factor of 21 at UV (360 nm). The side and top views (taken at the center) of the $|E_{norm}|^2$ of the UV mode are depicted in (a) and (b), respectively.

confined cavity mode could be identified at higher emission wavelengths in the visible and NIR wavelengths. The formation of this mode entails that, unlike the omnidirectional radiation from an ensemble of randomly oriented UCNP, the emission from the UCNP nanocavity has higher spatial coherence and therefore can be more effectively delivered to a target.

In conclusion, we proposed a plasmonic nanocavity as a means to engineer the emission spectra of UC nanocrystals. Our nanocavity provides up to a 34-fold increase in emissions at the 360 nm centered UV spectral band. This improvement is attributed to the modified NIR absorption and local photonic density of states in the presence of the proposed nanocavity. Although our analysis is applied to the $NaYF_4$ core-shell nanocrystals codoped by Tm^{3+} and Yb^{3+}, the results presented are generic. The proposed approach can be utilized in a variety of UC systems by optimizing the cavity size, metallic tube thickness, and by choosing an appropriate metal for tubing. Similarly, this analysis is applicable for different spectral bands. Since in our geometry the nanoparticles are not in direct contact with the metal, quenching, which is generally considered the most pressing limitation in using plasmonics resonances for UC enhancement, is of no concern. The UC containing nanocavities as proposed in this Letter could be potentially useful in drug delivery and release at target applications [14].

References

1. N. Bloembergen, Phys. Rev. Lett. **2**, 84 (1959).
2. F. Auzel, Chem. Rev. **104**, 139 (2004).
3. F. Wang, R. Deng, J. Wang, Q. Wang, Y. Han, H. Zhu, C. Xueyuan, and X. Liu, Nat. Mater. **10**, 968 (2011).
4. F. Wang, D. Banerjee, Y. Liu, X. Chen, and X. Liu, Analyst **135**, 1839 (2010).
5. S. Fischer, J. C. Goldschmidt, P. Löper, G. H. Bauer, R. Brüggemann, K. Krämer, D. Biner, M. Hermle, and S. W. Glunz, J. Appl. Phys. **108**, 044912 (2010).
6. S. Schietinger, T. Aichele, H. Q. Wang, T. Nann, and O. Benson, Nano Lett. **10**, 134 (2010).
7. Q. C. Sun, H. Mundoor, J. C. Ribot, V. Singh, I. I. Smalyukh, and P. Nagpal, Nano Lett. **14**, 101 (2014).
8. H. Zhang, Y. Li, I. A. Ivanov, Y. Qu, Y. Huang, and X. Duan, Angew. Chem., Int. Ed. Engl. **49**, 2865 (2010).
9. A. Shalav, B. S. Richards, and M. A. Green, Sol. Energy Mater. Sol. Cells **91**, 829 (2007).
10. E. M. Purcell, Phys. Rev. **69**, 829 (1946).

11. S. Fischer, H. Steinkemper, P. Löper, M. Hermle, and J. C. Goldschmidt, J. Appl. Phys. **111**, 013109 (2012).
12. S. E. Ivanova, A. M. Tkachuk, A. Mirzaeva, and F. Pellé, Opt. Spectrosc. **105**, 228 (2008).
13. Q. Nie, X. Li, S. Dai, T. Xu, Z. Jin, and X. Zhang, J. Lumin. **128**, 135 (2008).
14. M. L. Viger, M. Grossman, N. Fomina, and A. Almutairi, Adv. Mater. **25**, 3733 (2013).